Bulgarian Journal of Physics vol. **51** (2024) 365–376

Doublet Type II Solar Radio Bursts: A Dive into Their Interplay with Flares and CMEs Across Solar Cycles 23 and 24

Charita Pant[1], **Bimal Pande**[1*], **Seema Pande**[1], **Alankrita Joshi**[2]

[1]Department of Physics, DSB Campus, Kumaun University Nainital, Uttarakhand, 263001, India
[2]Department of Electronics and Communication, Graphic Era (Deemed to be University), Dehradun, Uttarakhand, 248002, India
[*]Corresponding author Email: pandebimal@yahoo.co.in

Received: 15 August 2024
doi: https://doi.org/10.55318/bgjp.2024.51.4.365

Abstract. In this paper, a statistical study of doublet type II radio bursts i.e. first type II (type II_1) and second type II (type II_2) associated with flares and CMEs for solar cycle 23 & 24 is presented. We have considered radio rich CMEs that are accompanied by type-II radio bursts for our analysis. Our study spans a duration of 15 years extending from November 1997 to December 2015, including solar cycles 23 and 24. We have analyzed the key attributes of doublet type II radio bursts by utilizing the data available at Culgoora radio spectrograph. A comparative study of the association of both type II solar radio burts with flares and CMEs for solar cycle 23 & 24 has been undertaken. In solar cycles 23 & 24, the flares start before the start of both two types of radio bursts and CMEs start after the onset of radio bursts which suggests that the solar flare is a precursor to both the radio bursts and the subsequent CME. The flare triggers the acceleration of particles that lead to the radio bursts. CME speed and acceleration are negatively correlated with a correlation coefficient of $r = -0.57$ and $r = -0.72$, this suggests that as CME speed increases, deceleration increases in both solar cycles 23 & 24.

KEY WORDS: Flares, radio rich CMEs, solar radio bursts.

1 Introduction

Solar bursts are fascinating phenomena associated with solar activity, particularly with solar flares and coronal mass ejections. When a solar flare occurs, it releases a burst of electromagnetic radiation across various wavelengths, including radio waves. This burst of radio waves is known as a solar radio burst. There are different types of solar radio bursts, classified based on their frequency

range and characteristics. One such type is the Type II solar radio burst, which typically occurs in the frequency range of 20-150 MHz. These bursts are often associated with shock waves generated by the eruption of material from the solar atmosphere during a flare or a coronal mass ejection.

Type II bursts are distinctive because they exhibit a characteristic frequency drift over time. This drift is caused by the motion of the shock wave through the solar corona and interplanetary medium. As the shock wave moves outward from the Sun, it causes density enhancements in the surrounding plasma, which in turn affects the propagation of radio waves. This results in the observed frequency drift. These bursts are important for studying solar activity and its impact on space weather. By monitoring and analyzing solar radio bursts, scientists can gain insights into the dynamics of solar flares, coronal mass ejections, and their effects on the Earth's magnetosphere and ionosphere. Type II radio bursts are intimately linked with coronal mass ejections (CMEs), which are massive eruptions of plasma and magnetic field from the Sun's corona into interplanetary space. When a CME occurs, it often generates shock waves that propagate outward through the solar corona and into the interplanetary medium [1, 2]. These bursts serve as important indicators of solar activity and are crucial for understanding the dynamics of the solar atmosphere and its effects on space weather [3]. The foreshock region is the region immediately ahead of a shock wave in a plasma, where particles are accelerated and conditions are favorable for wave-particle interactions. Observations have shown that Type II radio bursts are commonly detected in the foreshock regions of CME-driven shocks, highlighting the importance of these regions for the generation of such bursts.

Many authors like, Gopalswamy et al. [4,5], Sharma et al. [6] and Shanmugaraju et al. [7] have provided an explanation of the type-II burst's complete characterization and how they are caused by either flares or CMEs. Erupting magnetic flux ropes, coronal loops, and soft X-ray jets are also thought to be the source of type-II radio bursts [8]. Type II radio bursts are also generated as multiples reported by Robinson et al. [9] and Gergely et al. [10] and multiple bands can belong to a single multiple type II in the dynamic spectrum. The abundance of multiple type II radio bursts were reported by Robinson et al. [9]. According to them the overall percentage of multiple type IIs among all the type IIs is 20%. One such type is doublet type II radio bursts. Doublet Type II radio bursts are a specific subtype of Type II solar radio bursts, characterized by their occurrence in pairs. Both bursts are typically associated with the same solar event, such as a single CME, but may result from different parts of the shock or from multiple shock fronts. The two bursts in the pair often have similar temporal and frequency drift characteristics, though there may be slight variations. These bursts frequently show fundamental(F) and harmonic(H) frequency structures. The split-band feature arises due to the differential acceleration of electrons by the shock wave as it propagates through the solar corona and interplanetary medium. The frequency of harmonic band is twice that of fundamental frequency. These radio waves

are discharged close to local plasma frequency or its harmonic [11]. The lower frequency emission is typically generated by electrons accelerated at the leading edge or front of the shock, while the higher frequency emission is produced by electrons accelerated behind the shock [12].

In the present paper, we have examined the temporal characteristics of flares and radio rich CMEs that are accompanied by type-II solar radio bursts. We have also focussed on the identification of the main drivers responsible for the occurrence of these radio bursts. The structure of this article is organized as follows: Section 2 gives the detail of data selection and validation. Statistical analysis part has been discussed in Section 3. Section 4 deals with discussion and conclusion.

2 Data Selection and Validation

In the present paper, we have focussed our analysis on radio rich CMEs i.e. those CMEs that are accompanied by type II solar radio bursts. For these radio rich CMEs, doublet type II radio bursts are reported for two consecutive solar cycles, i.e. solar cycle 23 and 24. Our study spans a duration of 15 years extending from November 1997 to December 2015, including solar cycles 23 and 24. In order to have a uniform data set, the doublet type two radio burst data have been taken from Culgoora radio spectrograph for solar cycles 23 and 24. Out of fundamental and harmonic bands of doublet type II solar radio bursts, we have used harmonic band data of the spectrum.

Following data sources that have been used for the analysis:

1. Data regarding doublet type II radio bursts is taken from Culgoora radio catalog https://www.sws.bom.gov.au/World_Data_Centre.
2. The DH-type II radio bursts data is downloaded from Wind/WAVES type-II online catalog http://cdaw.gsfc.nasa.gov/CME_list/radio/waves_type2.html.
3. Different properties of CMEs (speed, width, acceleration,location) are extracted from the online SOHO/LASCO CME catalog available at http://cdaw.gsfc.nasa.gov/CME_list supported by CDAW data centre.
4. Data regarding flares (start time, end time, peak time, flare class) is taken from GOES soft X-ray flare catalog available at http://www.ngdc.noaa.gov/stp/solar/solarflares.html.

For the selection of the harmonic band data, the time difference between the start of first type II and second type II should be less than 30 minutes.

On the basis of above criteria a total of 23 and 11 events have been selected for our study. A comparative study has been done for the temporal characteristics of these events for solar cycles 23 and 24. Table 1 and Table 2 show start time of flares, doublet type II radio bursts and CMEs for solar cycles 23 and 24. We

Table 1. Start time of flares, doublet type II radio bursts and CMEs of solar cycle 23

Date	Flare	First type II radio burst	Second type II radio burst	CME
971103	04:32:00	04:37:00	04:50:00	05:28:07
971104	05:52:00	06:00:00	06:08:00	06:10:05
980125	21:26:00	21:35:00	21:56:00	22:19:30
980423	05:35:00	05:40:00	05:43:00	05:55:22
980509	03:04:00	03:26:00	03:31:00	03:35:58
990611	01:05:00	00:39:00	00:49:00	01:26:49
991116	04:47:00	05:07:00	05:16:00	05:30:05
000212	03:51:00	04:03:00	04:12:00	04:31:20
000217	20:17:00	20:25:00	20:38:00	21:30:08
000327	06:37:00	06:46:00	06:49:00	07:31:20
001124	04:55:00	05:02:00	05:19:00	05:30:05
001125	00:59:00	01:07:00	01:14:00	01:31:58
020720	21:04:00	21:10:00	21:20:00	20:06:09
020723	00:18:00	00:29:00	00:34:00	00:42:05
021110	03:04:00	03:16:00	03:20:00	03:30:11
021219	21:34:00	21:39:00	21:44:00	22:06:05
021222	02:14:00	02:43:00	02:48:00	03:30:11
030527	22:56:00	23:06:00	23:11:00	23:50:05
040912	01:36:00	01:41:00	01:50:00	00:36:06
041110	01:59:00	02:07:00	02:18:00	02:26:05
050709	21:47:00	21:59:00	22:03:00	22:30:05
060430	01:33:00	01:38:00	01:49:00	02:06:04
061214	21:07:00	22:10:00	22:10:00	22:30:04

Table 2. Start time of flares, doublet type II radio bursts and CMEs of solar cycle 24

Date	Flare	First type II radio burst	Second type II radio burst	CME
110607	06:16:00	06:26:00	06:33:00	06:49:12
110802	05:19:00	06:08:00	06:17:00	06:36:05
110906	01:35:00	01:46:00	01:54:00	02:24:05
110906	22:12:00	22:19:00	22:36:00	23:05:57
120517	01:25:00	01:32:00	01:38:00	01:48:05
130411	06:55:00	07:02:00	07:10:00	07:24:06
131005	07:30:00	06:51:00	06:55:00	07:09:51
140106	08:00:05	07:47:00	07:53:00	08:00:05
140225	00:39:00	00:49:00	00:58:00	01:25:50
150505	22:05:00	22:12:00	22:18:00	22:24:05
151223	00:52:00	00:36:00	00:51:00	01:25:47

have concentrated on identifying the primary factors that are responsible for the formation of these first type II and second type II solar radio bursts.

Figure 1 shows fundamental and harmonic structure of doublet type-II solar radio bursts of the radio dynamic spectra taken from Culgoora Radio Spectrograph for an event that occurred on 6 September 2011.

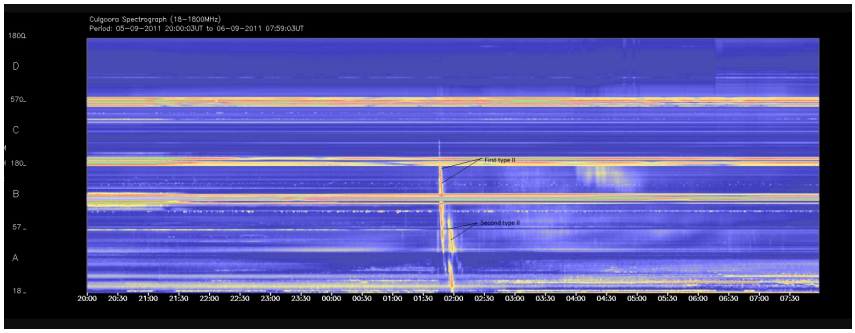

Figure 1. Radio dynamic spectrum from the Culgoora radio spectrograph showing doublet type II radio bursts. Two type II bursts can be seen in sequence, one starting at 1:46:00 UT and the second one at 1:54:00 UT on 6 Sep 2011. Both the bursts show fundamental/harmonic structure.

3 Statistical Analysis

3.1 Doublet type II radio burst associated flares

It is well known that flares and CMEs are responsible for causing DH and Km type II radio burst [5]. In the present paper, we have made an attempt to find whether doublet type-II radio bursts are caused by flares and CMEs. Table 3 and Table 4 show time difference between start of doublet type II_1 and type II_2 radio bursts and start of both the type of radio bursts & peak time of GOES X-ray flares for solar cycles 23 & 24.

Table 3. Time characterisitcs of doublet type II associated flares for solar cycle 23

Date	Time diff. between start of first type II & second type II	Time diff. between start of first type II & GOES X-ray flare	Time diff. between start of second type II & GOES X-ray flare	Time diff. between start of first type II & peak of GOES X-ray flare	Time diff. between start of second type II & peak of GOES X-ray flare
971103	13	5	18	12	1
971104	8	8	16	2	6
980125	21	9	30	8	13
980423	3	5	8	43	40
980509	5	22	27	29	24
990611	10	26	16	37	27
991116	9	20	29	38	29
000212	9	12	21	28	19
000217	13	8	21	42	29
000327	3	9	12	28	25
001124	17	7	24	6	11
001125	7	8	15	54	47
020720	10	6	16	44	34
020723	5	11	14	18	13
021110	4	12	16	19	15
021219	5	5	10	38	33
021222	5	29	34	29	24
030527	5	10	15	7	2
040912	9	5	14	0	9
041110	11	8	19	13	2
050709	4	12	16	20	16
060430	11	5	16	29	18
061214	0	3	3	16	16

Table 4. Time characterisitcs of doublet type II associated flares for solar cycle 24

Date	Time diff. between start of first type II & second type II	Time diff. between start of first type II & GOES X-ray flare	Time diff. between start of second type II & GOES X-ray flare	Time diff. between start of first type II & peak of GOES X-ray flare	Time diff. between start of second type II & peak of GOES X-ray flare
110607	7	10	17	33	26
110802	9	49	58	30	31
110906	8	11	19	19	11
110906	17	7	24	5	12
120517	6	7	13	42	36
130411	8	7	15	27	19
131005	4	39	35	47	43
140106	6	13	7	28	22
140225	9	10	19	14	5
150505	6	7	13	3	3
151223	16	13	18	16	1

The time difference between the start of first type II and second type II radio burst is shown in Figure 2 for solar cycles 23 and 24. The average values for this time difference for solar cycles 23 and 24 are 8 min and 9 min, respectively. Robinson et al. [9] also reported in his paper that the second type II radio burst starts 10 minutes after first type II radio burst by analyzing 145 multiple type II events from 1968 to 1981. Figure 3 shows time difference between the start of first type II and GOES X-ray flare and start of second type II and GOES X-ray flare for solar cycle 23 and solar cycle 24. For solar cycle 23, the time difference between the start of first type II and GOES X-ray flare is 5-8 minutes and the time difference between the start of second type II and GOES X-ray flare is 10–20 minutes and the respective time difference for solar cycle 24 is 7–15 minutes and 13–15 min, respectively. The mean time difference between the start of first type II and start of flare for solar cycle 23 is 11 min and mean time difference between the start of second type II and start of flare is 18 min and for solar cycle 24 it is 16 min and 22 min, respectively. The time difference between the start of type II_1 radio burst and peak of GOES X-ray flare and start of type II_2 radio burst and peak of GOES X-ray flare for solar cycle 23 and 24 is shown in Figure 4.

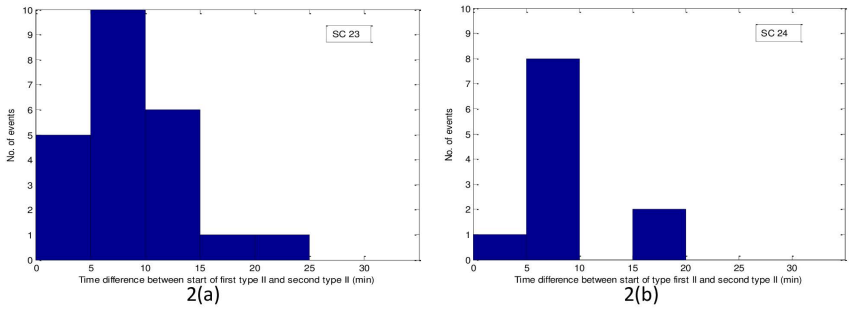

Figure 2. Comparison of the time difference between the start of first type II and second type II radio burst: (a) for SC 23; and (b) for SC 24.

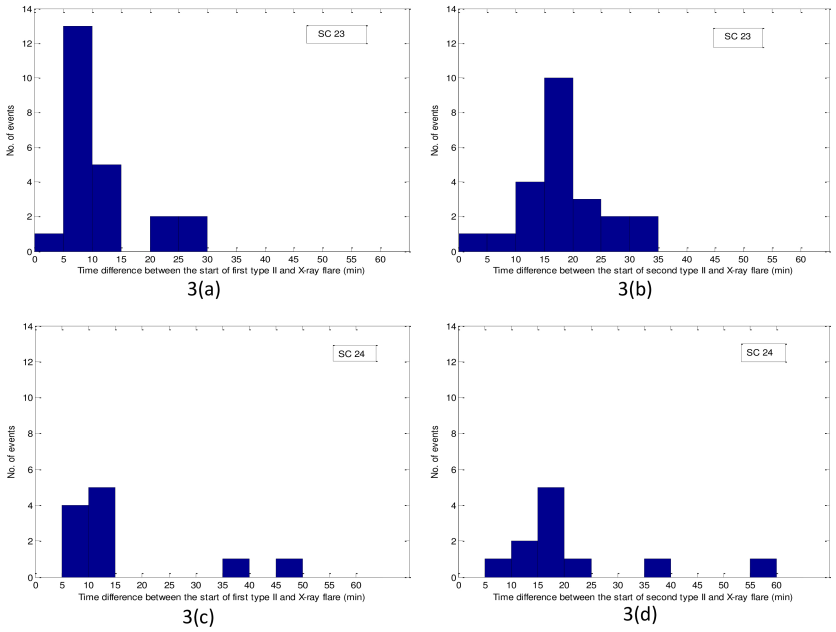

Figure 3. Comparison of the time difference between: (a) start of first type II and GOES X-ray flare for SC 23; (b) start of second type II and GOES X-ray flare for SC 23; (c) start of first type II and GOES X-ray flare for SC 24; (d) start of second type II and GOES X-ray flare for SC 24.

For solar cycle 23, the average value of time difference between first type II and peak of GOES X-ray flare is 24 min and between second type II and peak of GOES X-ray flare is 20 min. Similarly for solar cycle 24, the average value of time difference between first type II and peak of GOES X-ray flare and between second type II and peak of GOES X-ray flare is 24 and 19 min, respectively.

3.2 Doublet type II radio burst associated CMEs

CMEs are the main drivers responsible for the occurrence of doublet type-II radio bursts. The basic characteristics of CME is its mass motion and it is reflected by its speed. Occurence of CME results in the movement of leading edge towards greater heliocentric distance. One can measure CME height as a function of time by measuring the heliocentric distance of the leading edge of a CME in each LASCO image and thus the CME speed is measured by the height time plots projected in the sky plane and listed in the LASCO CME catalog [13]. There are 23 CME rich doublet type II radio burst events in solar cycle 23 and a total of 11 events in solar cycle 24. Figure 5 shows distribution of CME speed associated with doublet type II radio bursts for solar cycle 23 and 24. Most of

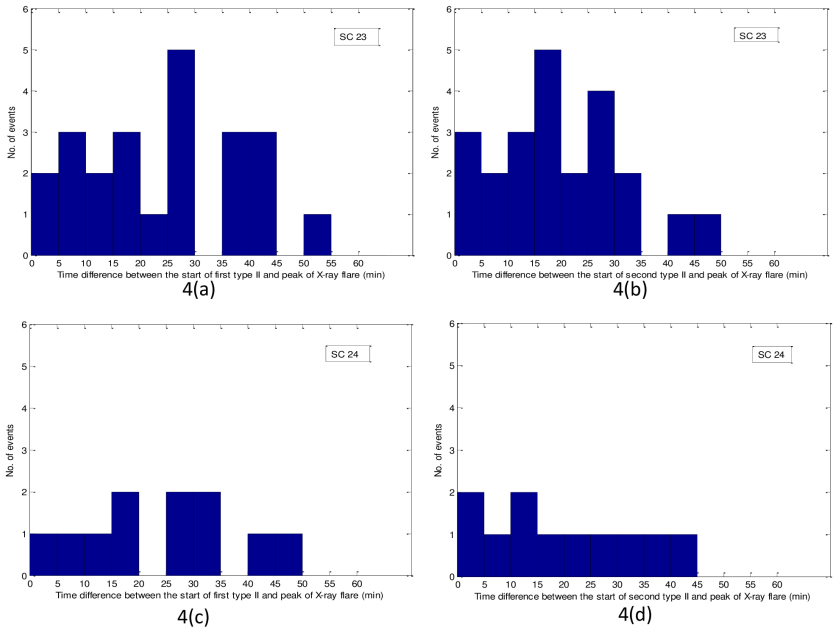

Figure 4. Comparison of the time difference between: (a) start of first type II and peak GOES X-ray flare for SC 23; and (b) start of second type II and peak GOES X-ray flare for SC 23; (c) start of first type II and peak GOES X-ray flare for SC 24; and (d) start of second type II and peak GOES X-ray flare for SC 24.

the doublet type II radio bursts associated with CME have their speed varying between 500–2500 km/s for both solar cycles. The mean CME speed during solar cycle 23 is 1304 km/s and that during solar cycle 24 is 1047 km/s. This reflects that CME speed is greater in solar cycle 23 than in 24. Our results are

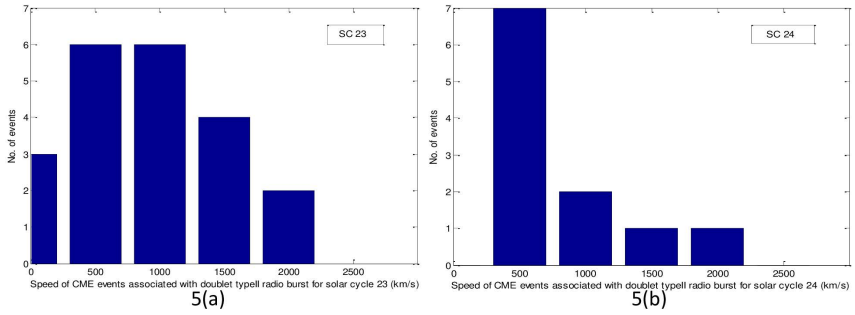

Figure 5. Comparison of speed of CME events associated with doublet type II radio burst: (a) for SC 23; and (b) for SC 24.

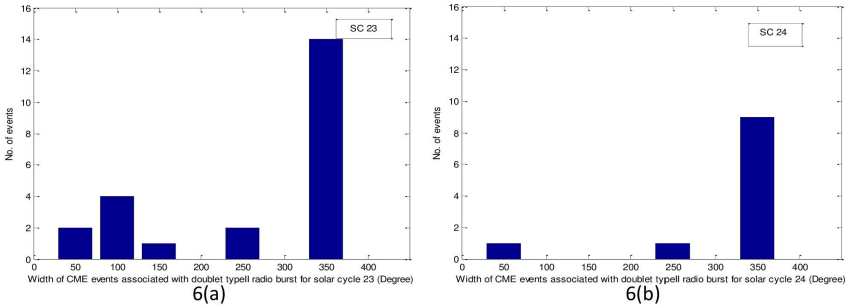

Figure 6. Comparison of angular width of CME events associated with doublet type II radio burst: (a) for SC 23; and (b) for SC 24.

in agreement with the results obtained by Bidhu et al. [14]. Since, release of magnetic energy from closed field regions are the main factors for CMEs to occur, therefore change in the behaviour of magnetic field structure and low total ambient pressure (magnetic and plasma pressure), could be the reason of higher CME speed in solar cycle 23.

The projected angular width is used to determine CME width. It is the span angle between the two position angles of the CME's outer edges relative to the Sun centre in the coronagraph's plane of sky. Figure 6 shows distribution of angular width of CMEs for solar cycle 23 and 24. About 61%(14/23) CMEs associated with doublet type II radio bursts are halo CMEs (having angular width 360°) for solar cycle 23 and about 82%(9/11) are halo CMEs for solar cycle 24. The maximum value of angular width ranges from 90 to 360 degree. Thus, we conclude that HCMEs are the main drivers of doublet type II radio bursts.

The acceleration or deceleration of CME as viewed in LASCO FOV depends on interaction with solar wind. Figure 7 shows distribution of CME acceleration

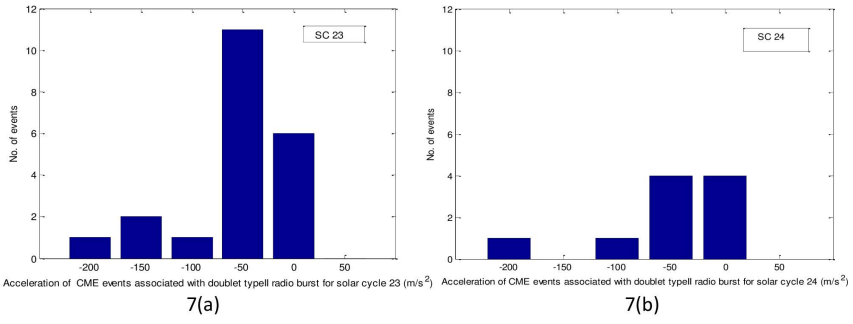

Figure 7. Comparison of acceleration of CME associated with doublet type II radio bursts: (a) for SC 23; and (b) for SC 24.

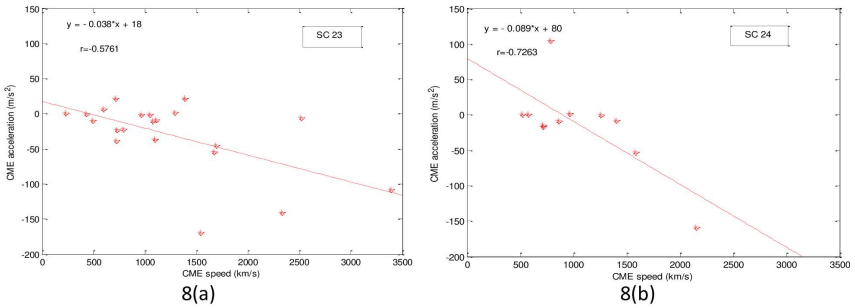

Figure 8. Correlation between CME speed and CME acceleration: (a) for SC 23; and (b) for SC 24.

for both solar cycles. In both cycles, larger no. of CMEs tend to decelerate. The mean acceleration for solar cycle 23 is -23 m/s^2 and that for solar cycle 24 is -13 m/s^2. The correlation between CME speed and acceleration for both solar cycle 23 and 24 is shown in Figure 8, respectively. There exist a good negative correlation, $r = -0.5761$ for solar cycle 23 and $r = -0.7263$ for solar cycle 24 between CME speed and CME acceleration. The acceleration/deceleration of CMEs is mainly because of Lorentz force. Yashiro et al. [13] also concluded in their paper that there is anticorrelation between CME acceleration and speed. Also several authors studied that CME acceleration increases with increase in speed [15]. However in our study due to aerodynamic drag [16, 17] acceleration decreases with increase in CME speed. As CMEs propagate through the interplanetary medium, the factor responsible for deceleration of CME is the drag force faced by these CMEs [18]. The dominant nature of this drag force over the dynamics of CMEs results in the decrease of Lorentz and gravity force and results in deceleration of CMEs occuring in LASCO FOV.

4 Discussion and Conclusions

In the present study, doublet type II radio bursts associated with flares and CMEs were analysed for solar cycles 23 and 24. In solar cycles 23 and 24, total no. of events that fit the selected criteria for the analysis are 23 and 11, respectively.

1. The average time difference between the onset of the first type II and the second type II radio bursts for solar cycle 23 is 8 minutes, while for solar cycle 24, it extends slightly to 9 minutes. Notably, our findings align closely with those reported by Robinson [9], who reported a mean time difference of 10 min for this temporal gap.
2. The mean time difference between the start of first type II and start of flare for solar cycle 23 is 11 min and mean time difference between the start of second type II and start of flare is 18 min and for solar cycle 24

it is 16 min and 22 min, respectively. Also, the average value of time difference between first type II and peak of GOES X-ray flare is 24 min and between second type II and peak of GOES X-ray flare is 20 min. Similarly for solar cycle 24, the average value of time difference between first type II and peak of GOES X-ray flare and between second type II and peak of GOES X-ray flare is 24 and 19 min respectively.

3. In both solar cycles 23 and 24, solar flares precede the occurrence of both type II_1 and type II_2 radio bursts, while Coronal Mass Ejections (CMEs) follow the onset of doublet type II radio bursts.
   This sequence implies that solar flares serve as a precursor to both the radio bursts and the subsequent CMEs. The flare's activity initiates particle acceleration, which leads to the radio burst, and it also signifies the association between flares and CMEs in the context of doublet type II radio bursts.
4. The mean CME speed during solar cycle 23 is 1304 km/s and that during solar cycle 24 is 1047 km/s. This reflects that CME speed is greater in solar cycle 23 than in 24. Our results are in agreement with the results obtained by Bidhu et al. [14].
   The release of magnetic energy from closed field regions primarily drives the occurrence of coronal mass ejections (CMEs). Consequently, alterations in the magnetic field structure and a decrease in total ambient pressure (comprising both magnetic and plasma pressure) likely contributed to the increased CME speeds observed during solar cycle 23.
5. About 61%(14/23) CMEs associated with doublet type II radio bursts are halo CMEs (having angular width 360°) for solar cycle 23 and about 82%(9/11) are halo CMEs for solar cycle 24. Thus, we conclude that HCMEs are the main drivers of doublet type II radio bursts.
6. In both solar cycles 23 and 24, there exists a negative correlation between CME speed and acceleration, with correlation coefficients of $r = -0.57$ and $r = -0.72$, respectively. This suggests that higher CME speeds correspond to increased deceleration. Such behavior can be attributed to the influence of the Lorentz force and the dominant nature of the aerodynamic drag force over CME dynamics.

Acknowledgement

We are thankful to the Culgoora Solar Radio Spectrograph team for their open data policy. We have used GOES and SOHO/LASCO data for X-ray flares and CMEs which is generated and maintained by the Centre for Solar Physics and Space Weather, Catholic University of America, in cooperation with the Naval Research Laboratory and NASA. One of the authors (B.Pande) is thankful for financial aid from Kumaun University internal research grant vide letter no. KU/RDC/IFR/2023-24/1127 dated 12/Feb/2024.

References

[1] O. Prakash, S. Umapathy, A. Shanmugaraju, B. Vrsnak (2009) Type II bursts in meter and Decameter-Hectometer wavelength ranges and their relation to flares and CMEs. *Solar Phys*. **258** 105-118.

[2] N. Gopalswamy, E.A. Rodriguez, S. Yashiro, S. Nunes, M.L. Kaiser, R.A. Howard (2005) Type II radio bursts and energetic solar eruptions. *J. Geophys. Res. Space Phys.* **110** A12S07(1-15).

[3] A. Nindos, H. Aurass, K.L. Klein, G. Trottet (2008) Radio Emission of flares and Coronal mass ejections. *Solar Phys.* **253** 3-41.

[4] N. Gopalswamy, Y. Hanaoka, T. Kosugi, R.P. Lepping, J.T. Steinberg, S. Plunkett, R.A. Howard, B.J. Thompson, J. Gurman, G. Ho, N. Nitta, H.S. Hudson (1998) On the relationship between coronal mass ejections and magnetic clouds. *Geophys. Res. Lett*. **25**(14) 2485-2488.

[5] N. Gopalswamy (2000) Type II solar radio bursts. Radio Astronomy at long Wavelengths. *Geophysical Monogr. Ser*. **119** 123-135.

[6] J. Sharma, N. Mittal, V. Tomar, U. Narain (2008) On properties of radio-rich coronal mass ejections. *Astrophys. Space Sci*. **317** 261-265.

[7] A. Shanmugaraju, Y.J. Moon, K.S. Cho, Y.H. Kim, M. Dryer, S. Umapathy (2005) Multiple type II solar radio bursts. *Solar Phys*. **232**(1-2) 87-103.

[8] A. Klessen, S. Pohjolainen, K.L Klein (2003) Type II radio precursor and X-ray flare emission. *Solar Phys*. **218** 197-210.

[9] R.D. Robinson, K.V. Sheridan (1982) A study of multiple type II solar radio events. *Astronomical Society of Australia, Proceeding* **4**(4) 392-396.

[10] T.E. Gergely, M.R. Kundu, S.T. Wu, M. Dryer, Z.K. Smith, R.T. Stewart (1984) A multiple type-II burst associated with a coronal transient and its MHD simulation. *Adv. Space Res*. **4**(7) 283-286.

[11] J. Sharma, N. Mittal (2017) On high and low starting frequencies of type II radio bursts. *Astrophys*. **60** 213-222.

[12] S.F. Smerd, K.V. Sheridan, R. Stewart (1974) On Split-Band Structure in Type II Radio Bursts from the Sun. *Astrophys. Lett*. **57** 389-393.

[13] S. Yashiro, N. Gopalswamy, G. Michalek, O.C. St.Cyr, S.P. Plunkett, N.B Rich, R.A. Howard (2004) A catalog of white light coronal mass ejections observed by the SOHO spacecraft. *J. Geophys. Res*. **109** A07105(1-11).

[14] S.S. Bidhu, I.A. Sobia, D.A. Benjamin (2017) CME speed and angular width distributions during 23 and 24 solar cycle maximum. *J. Space Expl.* **6**(1) 122-126.

[15] N. Gopalswamy, S. Yashiro, M.L. Kaiser, R.A. Howard, J.L. Bougeret (2001) Characteristics of coronal mass ejections associated with long-wavelength type II radio bursts. *J. Geophys. Res. Space Phys*. **106**(A12) 29219-29229.

[16] B. Vrsnak (2001) Deceleration of Coronal Mass Ejections. *Solar Phys*. **202**(1) 173-189.

[17] B. Vršnak (2001) Onset of metric and kilometric type II bursts. In: "*The Dynamic Sun, Proceedings of the Summerschool and Workshop held at the Solar Observatory Kanzelhöhe, 1999*" edited by A. Hanslmeier), Mauro Messerotti, Astrid Veronig. Springer Netherlands, pp. 255-258.

[18] B. Vršnak, D. Ruždjak, D. Sudar, N. Gopalswamy (2004) Kinematics of coronal mass ejections between 2 and 30 solar radii. *Astron. Astrophys.* **423**(2) 717-728.